

Reliability of Boost PFC Converters with Improved EMI Filters

Haoqi Zhu, Dongliang Liu *, Xu Zhang and Feng Qu

College of Automation, Hangzhou Dianzi University, Hangzhou 310018, China; hqzhu23@163.com (H.Z.); ZX_HDU@163.com (X.Z.); qfeng137@163.com (F.Q.)

* Correspondence: liudl@hdu.edu.cn; Tel.: +86-18767187825

Received: 9 November 2018; Accepted: 4 December 2018; Published: 8 December 2018

Abstract: The switching device in a power converter can produce very serious electromagnetic interference (EMI). In order to solve this problem and the associated reliability and stability issues, this article aimed to analyze and model the boost power factor correction (PFC) converter according to the EMI conduction path. The sources of common-mode (CM) and differential-mode (DM) noise of the boost PFC converter were analyzed, and the DM and CM equivalent circuits were deduced. Furthermore, high-frequency modeling of the common-mode inductor was developed using a precise model, and the EMI filter was designed. According to the Class B standard for EMI testing, it is better to restrain the EMI noise in the frequency range (150 kHz to 30 MHz) of the EMI conducted disturbance test. Using this method, a 2.4-kW PFC motor driving supply was designed, and the experimental results validate the analysis.

Keywords: common-mode inductor; high-frequency modeling; electromagnetic interference; filter

1. Introduction

With the rapid development of electronic technology, power converters are widely used in various fields [1]. The application of the product requires the power to be converted to maintain high reliability and stability. In order to pursue higher performance and smaller size, the switching frequency of power devices is becoming increasingly higher [2,3]. With the continuous improvement of the switching frequency in power devices, its reliability became a common and urgent problem that needs to be solved. The reliability of the power converter is affected by the manufacturing process and actual operating conditions.

Scholars from various countries conducted extensive research on the reliability of converter devices and their power devices [4–6]. Power converters usually consist of switching devices, storage devices, driving devices, and signal processing and control circuits. The reliability of the converter is determined comprehensively by the reliability of each part. All kinds of capacitive elements, especially aluminum electrolytic capacitors, are key factors which affect the reliability of power converters. However, research shows that the power switching device is the most likely part to lose efficacy among the components of the converter. As the most fragile component of the power electronic switching device, the reliability of the power switching device determines the reliability of the entire device to some extent. Studying the reliability of power devices is the basis for improving the reliability of power converters [7]. The discussion of reliability in this paper is based on the influence and suppression of the interference caused by power converters in actual operation. When the device is operated beyond the rated voltage or current range, it may cause excessive electrical stress and damage to the power device [8,9]. Under excessive electrical stress, part of the device will locally overheat. When the hot-spot temperature reaches the melting point of the material, the material will melt, causing damage to the device. When the circuit interference is relatively strong,

the disturbance will form a strong inrush current through the parasitic parameters in the circuit, which will cause the power device (diode, rectifier bridge, metal-oxide-semiconductor field-effect transistor (MOSFET), etc.) to be damaged. The power switching device has a high current voltage, which causes great switching loss and strong interference. The rapidly changing dI/dt and dV/dt of the power device causes a strong interference current through the parasitic parameters in the circuit, which influences the reliability and stability of the power converter [10]. The interference current caused by the power device is mainly the common-mode (CM) current, which is the conduction interference in the converter. This can be suppressed by an electromagnetic interference (EMI) filter. Therefore, the conduction interference in the circuit of the power converter needs to be analyzed and suppressed in order to improve its reliability and stability.

Because current power converters are widely used, the electromagnetic compatibility (EMC) problem became increasingly important, a serious problem of which is the EMI [11]. The conducted interference and radiation interference need to be suppressed for correct functioning of the power converter. The radiated EMC effect of the power converter was introduced in Reference [12], and magnetic dipole array-based time-domain (TD) modeling of the electromagnetic near-field (NF) using a printed circuit board (PCB) was presented. Modeling of metallic wire susceptibility to the disturbances caused by electromagnetic near-field radiation by electronic structures in radio frequencies was introduced to suppress radiated EMC coupling of a power converter in Reference [13]. Furthermore, scholars also studied the influence of temperature and bandwidth on a power converter's lumped components [14]. These studies are helpful for the suppression of EMC in power converters.

The noise between the power converter system and ground is known as CM noise, and two power transmission paths are called differential-mode (DM) noise. In order to limit the EMI noise, a series of EMC standards were developed. These standards define the frequency range and the maximum amplitude of the allowable EMI noise. EMI filters are usually added to the circuit in order to solve the EMI issue. Analysis of EMC is based on three factors: jamming source, coupling path, and disturbed object. EMI filters can reduce the interference signal, cut off or change the propagation path of a jamming signal, and increase the anti-jamming ability of the disturbed object. For restraining the conduction EMI of power converters, we start with reducing the interference source and changing the conduction path.

Boost power factor correction (PFC) converters are widely used; thus, this paper investigated the use of boost PFC converters [15–18]. Firstly, the EMI of the boost PFC converter needed to be analyzed. The switch drain source voltage of the boost PFC converter was considered as the EMI source. According to the EMI conduction path, the causes of CM and DM interference were analyzed. The boost PFC's DM and CM equivalent circuits were derived. For the conduction interference in the circuit, an appropriate EMI filter circuit was selected. In addition, the high-frequency modeling of the common-mode inductor was analyzed in the circuit, which effectively suppressed the EMI. Finally, an EMI filter based on the improved CM inductor was designed for a PFC motor drive application. The experimental and commercial test results are presented, and the superiority of the proposed EMI filter and the reliability of the boost PFC converter are verified.

2. EMI Analysis of the Boost PFC

Due to the strong EMI found in the PFC boost circuit during testing, it affected the normal operation of the circuit. Therefore, we needed to analyze the conduction interference in the circuit. The conduction EMI of the boost PFC converter can be analyzed from two aspects: DM interference and CM interference. The DM current is transmitted between two wires, which is independent of the ground wire. The amplitude and phase of the two wires are the same, and the interference voltage is formed on the signal line. Through the parasitic capacitance of the interference source, the CM current is introduced into the ground along the ground transmission from the signal line return, where the same amplitude and phase opposite in each wire and ground, at the same time, form the interference voltage. When the impedance of two wires in the converter is unbalanced, the distribution of the CM

current is different between two conductors. Thus, the CM noise becomes the DM noise to some extent.

The drain source voltage (V_{DS}) of the power devices of the boost PFC converter can be considered as the noise voltage source of the CM and DM interferences. It is generally considered that the DM current is mainly caused by the ripple current of the inductor, and the CM current flows mainly from the drain electrode of the switch tube and the parasitic capacitor of the protector, as shown in Figure 1.

When the current of the inductor L_0 is discontinuous, the junction capacitance of inductor L_0 , the switching device, and the rectifier bridge D_1 – D_4 will induce resonance. The input voltage, after being rectified, will produce voltage spikes that will not only damage the rectifier bridge and switching devices, but also cause common-mode interference. Therefore, the DM capacitor C_{X1} is usually added behind the rectifier bridge to suppress the voltage spike. At this point, since the capacitance value of differential-mode capacitor C_{X1} is larger than the junction capacitance value of the rectifier diode and the switch tube, the voltage of capacitor C_{X1} remains substantially constant when the inductor current is discontinuous. When the rectifier bridge is on, the DM capacitor provides a low-impedance path for the L and N lines, which suppresses the differential-mode interference. If without capacitor C_{X1} , due to impedance imbalance in the circuit, some of the DM current in the boost PFC converter is generated by the CM current.

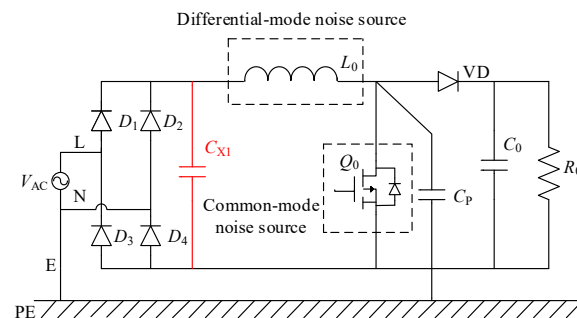
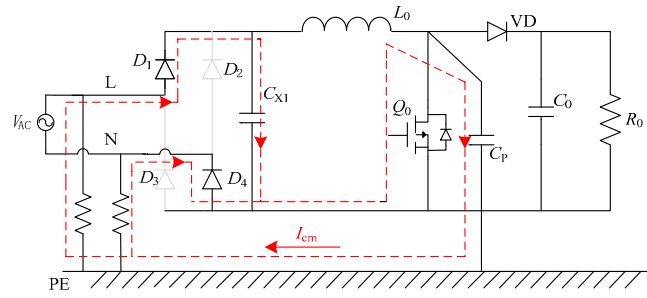
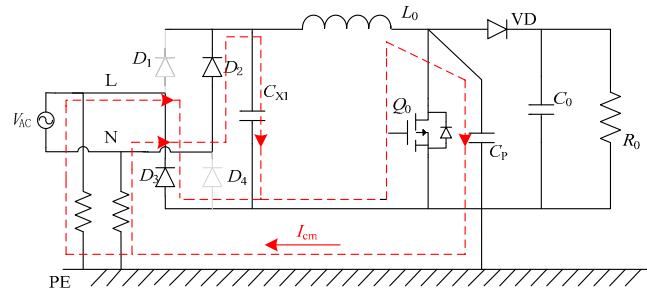
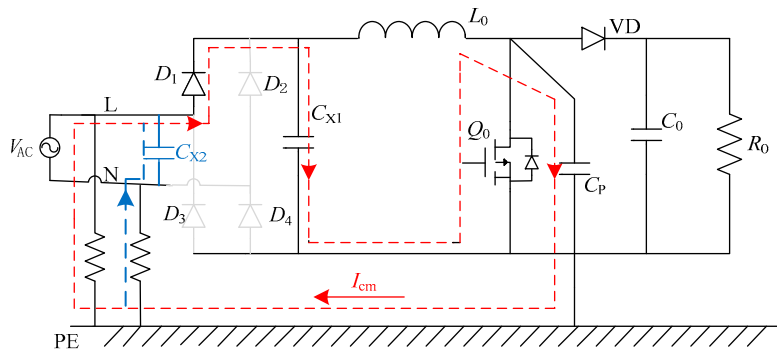
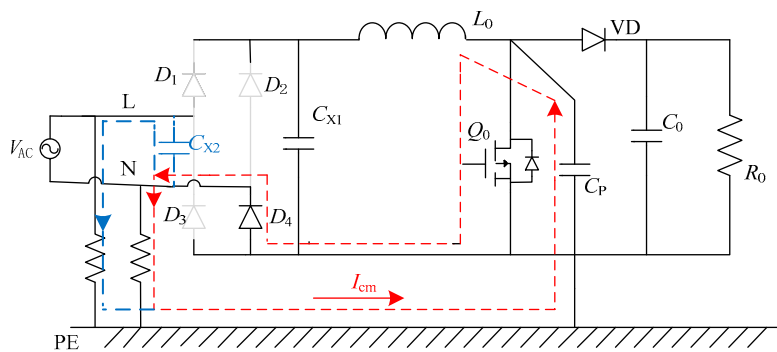


Figure 1. Common-mode (CM) and differential-mode (DM) interference sources in the boost power factor correction (PFC) converter.

When the rectifier bridge is on, due to the DM capacitance C_{X1} , the CM current from the chassis almost meets the equivalent impedance. At this time, the CM noise almost equally flows into the L and N lines, where we avoid the CM interference transformation position difference caused by the line impedance unbalance. As shown in Figure 2, the diodes in grey do not conduct. When the input voltage is positive, D_1 and D_4 conduct; however, the noise reversely flows through diode D_4 because the alternating current (AC) power grid voltage makes the diode conduct. In the negative half-cycle, D_2 and D_3 will conduct, and a similar analysis can be performed. The addition of C_{X1} will result in harmonics of the input current and needs to ensure that the frequency is higher than 150 kHz. A C_{X1} capacity resistance that is much less than 50 Ω can effectively suppress the mixed interference (the DM interference in part from the CM interference).

As shown in Figure 3, the rectifier bridge is off and the CM current passes the test resistor on the L line and D_1 , which produces the interference voltage. Obviously, when the CM current does not flow through the L-line and N-line resistors, the DM voltage is generated. In order to inhibit the problem caused by the impedance imbalance, a DM capacitor can be added.

(a) D_1 and D_4 turn on(b) D_2 and D_3 turn on**Figure 2.** Common-mode current path.(a) D_1 turn on (C_P charging)(b) D_4 turn on (C_P discharging)**Figure 3.** Common-mode current when the rectifier bridge is off.

3. Boost PFC CM and DM Equivalent Circuits

In Figure 4, the CM and DM interference paths of the boost PFC converter are given, where the capacitors C_{X1} and C_{X2} are added according to the above discussion. The green dotted line represents the DM interference path, and the red dashed line represents the CM interference path.

$$V_{CM} = \frac{V_{DS} \cdot \pi f C_P R_{LN}}{\sqrt{(\pi f C_P R_{LN})^2 + 1}} \quad (1)$$

$$V_{DM} = \frac{V_{DS} \cdot R_{LN}}{2\sqrt{R_{LN}^2(4\pi^2 f^2 L C_X - 1)^2 + 16\pi^2 f^2 L^2}} \quad (2)$$

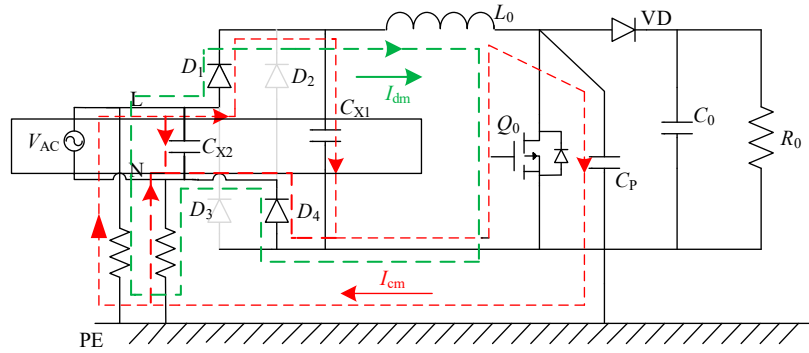
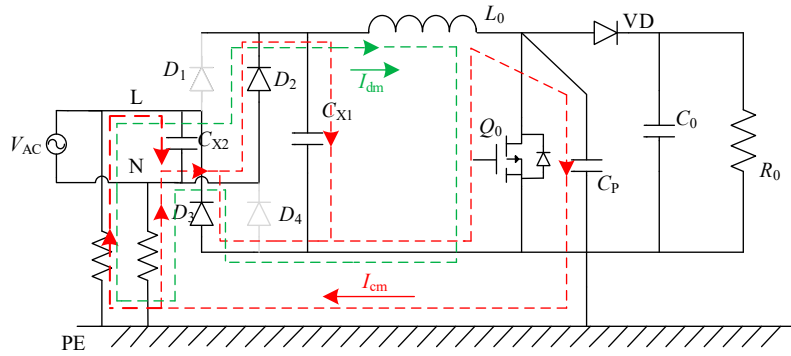
(a) D_1 and D_4 are on(b) D_2 and D_4 are on

Figure 4. Electromagnetic interference (EMI) paths when the rectifier bridge is on with the filter capacitors.

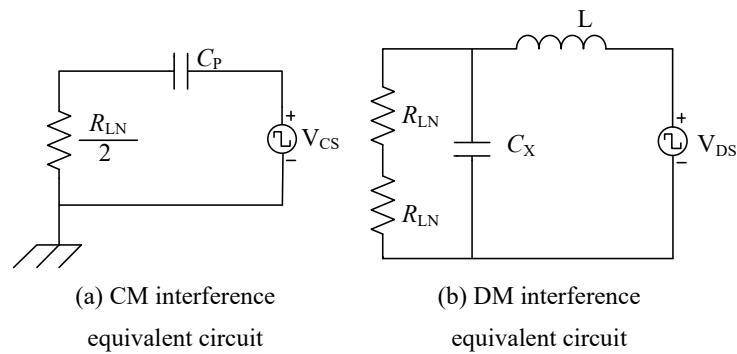


Figure 5. Common-mode and differential-mode equivalent circuits of the boost PFC converter.

Figure 5 shows the CM and DM equivalent circuit of the boost PFC converter. According to Figure 4, the filter capacitors C_{X1} and C_{X2} are parallel. Make $C_X = C_{X1} + C_{X2}$. In the CM interference branch, C_X is connected in series with the test resistor R_{LN} on the branch. When the impedance of C_X is smaller than the test resistance R_{LN} , it can be considered that the filter capacitor C_X is short-circuited, and the test resistance of the L and N lines is equivalent to the parallel connection. Therefore, the test resistance on the CM interference equivalent circuit is $R_{LN}/2$, and its CM interference voltage is V_{CM} .

The CM interference equivalent circuit is shown in Figure 5a. The transmission gain $|TG_{CM}(f)|$ of the CM voltage is derived as below.

$$|TG_{CM}(f)| = \left| \frac{R_{LN}}{R_{LN} + \frac{2}{j2\pi f C_P}} \right| = \frac{\pi f C_P R_{LN}}{\sqrt{(\pi f C_P R_{LN})^2 + 1}}. \quad (3)$$

Due to the parasitic capacitance C_P in the circuit, generally, $\pi f C_P R_{LN} \ll 1$, and the amplitude of the CM interference voltage is derived as below.

$$V_{CM} = V_{DS} \times |TG_{CM}(f)| = V_{DS} \times \pi f C_P R_{LN}. \quad (4)$$

Obviously, with the increase of frequency f , the CM interference voltage V_{CM} will increase at a slope of 20 dB/dec. The parasitic capacitance has an obvious influence on CM interference.

Meanwhile, the decrease of voltage V_{DS} will reduce the CM interference.

In the DM interference branch, the DM current flows through the test resistor R_{LN} of the L and N lines in sequence. Therefore, the test resistance on the DM interference equivalent circuit is $2R_{LN}$, and the DM interference voltage is V_{DM} . The DM interference equivalent circuit is shown in Figure 5b. The transmission gain $|TG_{DM}(f)|$ of the CM voltage is derived as below.

$$|TG_{DM}(f)| = \left| \frac{2R_{LN} // \left(\frac{1}{j2\pi f C_X} \right)}{2R_{LN} // \left(\frac{1}{j2\pi f C_X} \right) + j2\pi f L} \right| = \frac{R_{LN}}{2\sqrt{R_{LN}^2 (4\pi^2 f^2 L C_X - 1)^2 + 16\pi^2 f^2 L^2}}. \quad (5)$$

Usually, when the frequency f is higher than 150 kHz, $4\pi^2 f^2 L C_X \gg 1$ and $4\pi^2 f^2 L C_X R_{LN} \gg \pi f L$. The amplitude of the DM interference voltage is derived as below.

$$V_{CM} = V_{DS} \times |TG_{DM}(f)| = V_{DS} \frac{1}{8\pi^2 f^2 L C_X}. \quad (6)$$

Obviously, with the increase of frequency f , the DM interference voltage V_{DM} will decline at a slope of -40 dB/dec. Meanwhile, it can be seen from the formula that, in the boost PFC converter, increasing the boost inductor can obviously reduce the DM interference, and decreasing the rate of the up or down of switching devices can reduce the DM interference.

From the above analysis, for the DM and CM interferences, the noise source is the switching device. The DM interference will be converted into CM interference. The parasitic parameters of the boost PFC converter have an impact on the DM and CM interferences. However, the influence is different. The boost inductance mainly affects the DM interference, and the parasitic capacitance between the switching device and the radiator shell mainly affects the CM interference.

4. Model of the CM Inductor and EMI Filter Design

4.1. The High-Frequency Model of CM Inductor

Since the common-mode inductor can achieve a very large inductance value in a very small magnetic core, it is widely used in EMI filters, as it can restrain EMI's common-mode noise interference very well. In the EMI conduction frequency range, the CM inductor will be affected by the leakage inductance and various parasitic parameters when working at high frequencies, such that its characteristics will change nonlinearly with the frequency. In order to improve the design of EMI filters and to accurately select a common-mode inductor, it is necessary to establish a suitable common-mode inductor high-frequency model in the EMI interference frequency range.

The CM model is more complex, and because of the nonlinearity of the magnetic element, the parameters of the common-mode equivalent model vary with the frequency [19–21]. Based on these reasons, a more complex model was used to characterize the high-frequency modeling of CM inductors. The improved model, shown in Figure 6, was based on the traditional Foster model [22]. The first level mainly consisted of the core characteristics (influence of iron core, layer number, and turn number), the second level determined the position and amplitude of the second resonant peak, and the third level determined the phase frequency characteristics before and after the second

resonance peak, in which stray capacitance C_1 is mainly related to the lead length of the common-mode inductor. The n -order Foster model can be expressed by n -harmonic peaks.

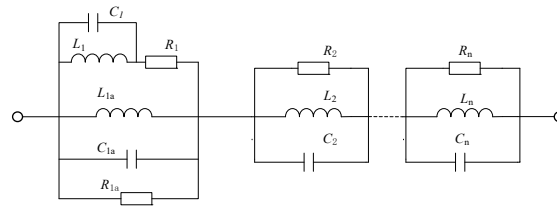


Figure 6. Common-mode inductor high-frequency model.

In order to verify the feasibility of the model, an impedance analyzer was used to test the CM inductance sample, and the scanning frequency range was 150 kHz to 30 MHz. Figure 7 shows the comparison results, fitted using MATLAB.

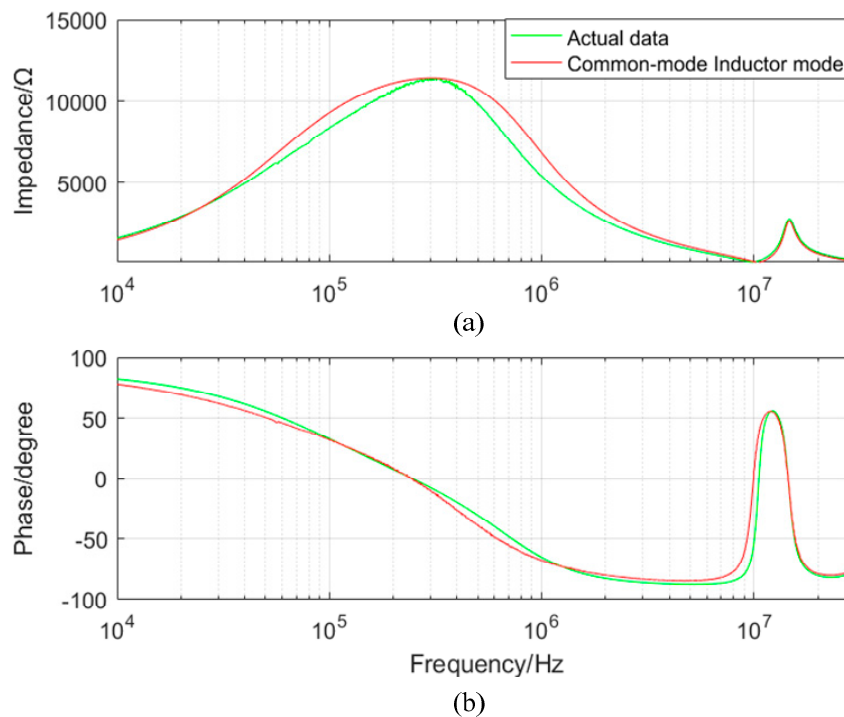


Figure 7. MATLAB fitting comparison.

According to the simulation results in Figure 7, the high-frequency model of the CM inductor (see Figure 6) in this paper had a better fitting effect both in impedance (see Figure 7a) and in phase (see Figure 7b). Thus, the model circuit shown in Figure 6 can reflect the change of the CM impedance in the frequency range of 10 kHz to 30 MHz. This improved model is suitable for all kinds of power converters with EMI filters, for example, PFC boost converters, bridgeless converters, and so on.

4.2. EMI Filter Design

The EMI filter's attenuation of conducted EMI can be expressed as the voltage insertion gain. The voltage insertion gain is defined as the ratio of the interference voltage measured before and after adding the EMI filter. Similarly, CM and DM equivalent circuits of the EMI filter need to be established, and then the CM and DM attenuation effects of the filter are considered, respectively. The filtering effect of EMI filters is not only related to its own parameters, but is also closely related to interference source impedance. Therefore, in order to design EMI filters efficiently, it is necessary to choose an appropriate filter topology according to different impedance characteristics. In medium

and high power of the converters, due to strong common-mode interference, two-stage EMI filters are usually used to suppress interference. In general, the leakage inductance of a CM inductor is used as a DM inductor when designing an EMI filter. Figure 8 shows the two-stage EMI filter topology. In Figure 8, C_{Y1} and C_{Y2} are CM capacitors and their values are equal, C_{X1} – C_{X3} are DM capacitors, and L_{CM1} and L_{CM2} are CM inductors.

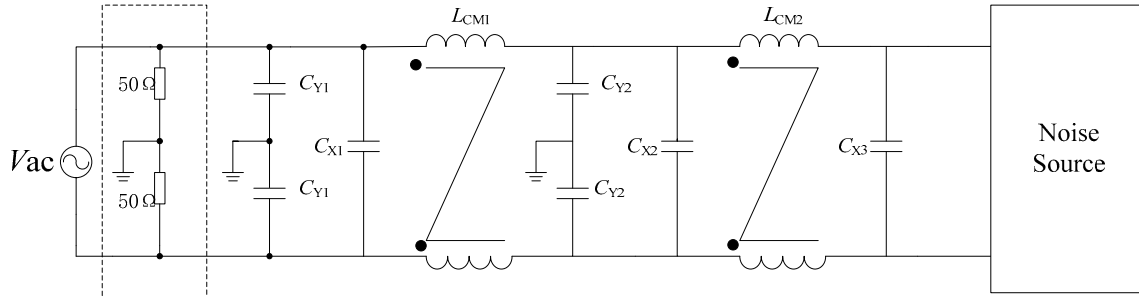


Figure 8. The EMI filter topology.

The attenuation of an EMI filter can be represented by the voltage insertion gain. The common-mode equivalent circuits are shown in Figure 9. The differential-mode equivalent circuits are shown in Figure 10.

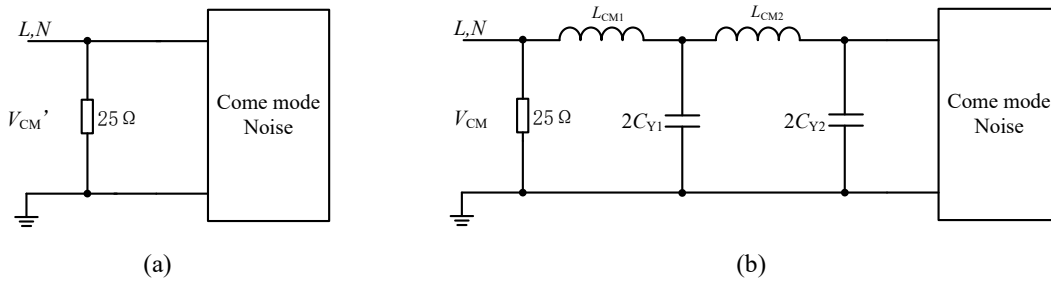


Figure 9. Common-mode equivalent circuits.

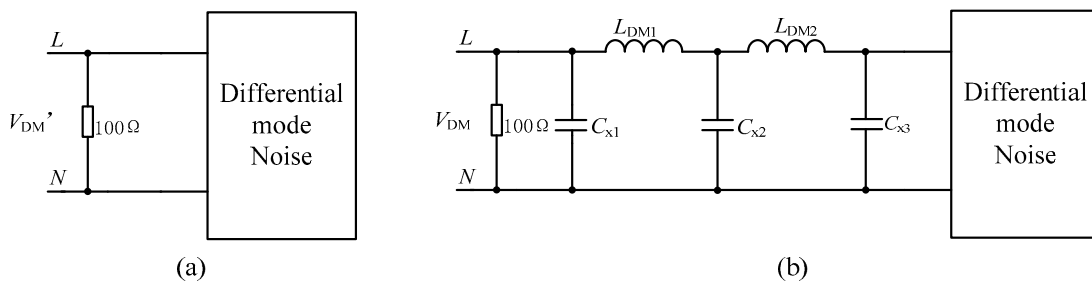


Figure 10. Differential-mode equivalent circuits.

The attenuation can be exemplified by the common-mode equivalent circuit. The CM interference voltage is V'_{CM} when the filter is not added, and the CM interference voltage is V_{CM} when the filter is added. Therefore, the CM insertion gain is derived as below.

$$\begin{aligned}
 G_{CM}(s) &= \frac{V'_{CM}}{V_{CM}} \\
 &= \frac{L_{CM1}L_{CM2}2C_{Y1}2C_{Y2}s^4 + L_{CM2}2C_{Y1}2C_{Y2}R_{CM}s^3}{[L_{CM2}2C_{Y1} + 2L_{CM1}(C_{Y1} + C_{Y2})]s^2} \\
 &\quad + 2R_{CM}(C_{Y1} + C_{Y2})s + 1.
 \end{aligned} \tag{7}$$

Figure 11 shows a simplified common-mode equivalent model. According to Equations (8)–(11), the insertion loss of the common mode can be calculated.

$$Z_{CM1} = R + Z_{L1}; \quad (8)$$

$$Z_{CM2} = Z_{L2} + Z_{Y1} \times \frac{Z_{CM1}}{Z_{Y1} + Z_{CM1}}; \quad (9)$$

$$G_{CM} = (Z_{Y2} + Z_{CM2}) \times \frac{Z_{Y1} + Z_{CM1}}{Z_{Y1} + Z_{Y2}}; \quad (10)$$

$$I_L = 20 \log_{10} \sqrt{(Re|G_{CM}|)^2 + (Im|G_{CM}|)^2}. \quad (11)$$

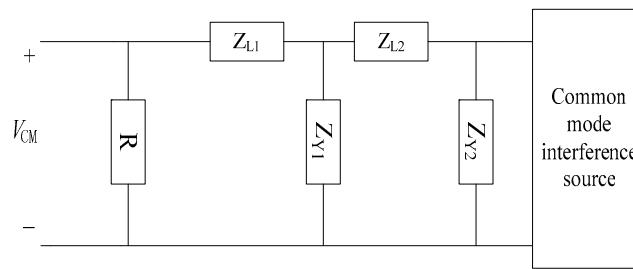


Figure 11. Common-mode equivalent circuit simplified diagram.

According to the previous analysis of the boost PFC circuit and the high-frequency modeling of the common-mode inductor, the high-frequency attenuation performance of the EMI filter can be evaluated more accurately. Meanwhile, it will better suppress the interference of the boost PFC circuit, which helps the reliability of power converters.

5. Experimental Results

Based on the above analysis, the EMI filter was designed, and the boost PFC converter was optimized. The experimental platform of a 2.4-kW boost PFC motor was built, and the experimental prototype is shown in Figure 12a. Figure 12b is the experimental EMI test platform. Figure 12c shows the input voltage and input current waveforms of the boost PFC converter system. Figure 12d shows the output voltage waveforms. Figure 13 shows the EMI conduction test results of the experimental prototype. Clearly, as shown in Figure 13, the 2.4-kW boost PFC test platform could successfully pass the EMI test. The power factor (PF) of the prototype was very high, and the system could run stably for a long time, thus ensuring the security, reliability, and stability of the system.

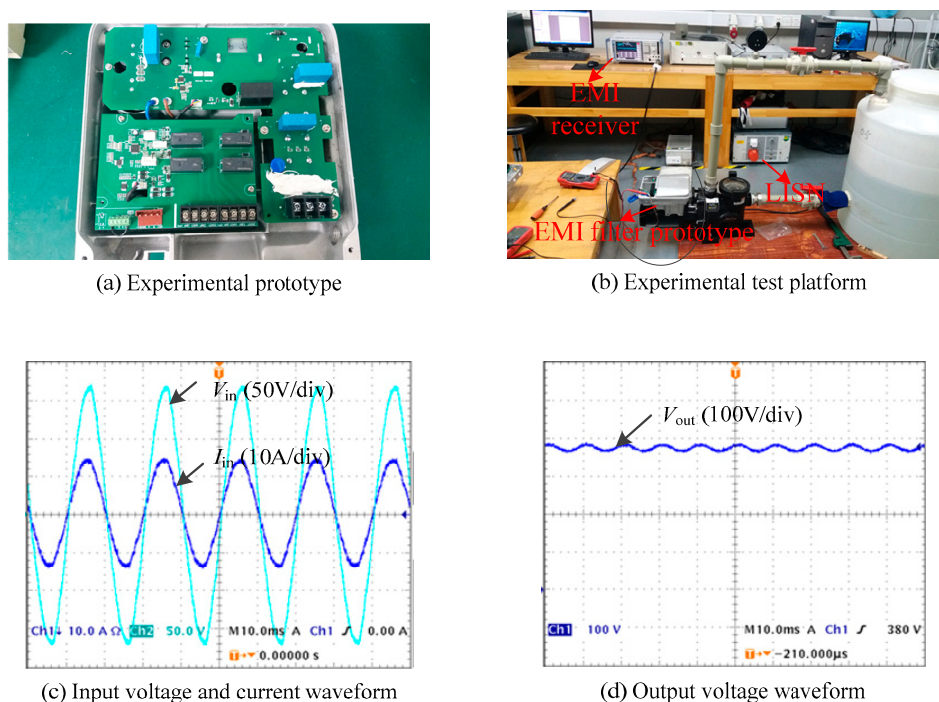


Figure 12. Experimental results.

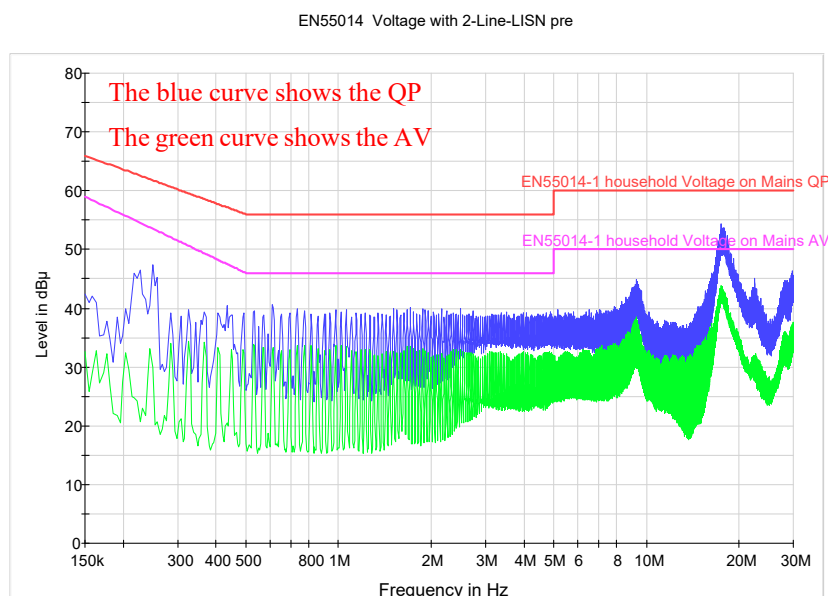


Figure 13. EMI conduction test results.

6. Conclusions

A boost PFC converter can be used to analyze and suppress the EMI issue of power converters. Here, CM and DM interferences of the boost PFC converter were analyzed and discussed in detail. To alleviate the EMI challenges in the reliability of the entire converter system, a common-mode inductor was designed accordingly and modeled. Using MATLAB simulations, it was found that the improved model, based on the traditional Foster model, could better represent the impedance/frequency characteristics of the common-mode inductor. In addition, the design of the EMI filter could better suppress the CM and DM interferences of the boost PFC converter. EMI-conducted interference could be suppressed using this method. Thus, the reliability of the boost PFC converter was improved. Finally, both simulation results and experimental tests validated the analysis and results.

Author Contributions: H.Z. and D.L. conceived the main idea, performed the testing and data analysis, and wrote the manuscript. X.Z. and F.Q. gave suggestions and contributed with data processing.

Funding: This research received no external funding.

Acknowledgments: The authors are particularly grateful to the team of Guozhu Chen of Zhejiang University for their help.

Conflicts of Interest: The authors declare no conflicts of interest.

References

1. Yuan, Y.-S.; Qian, Z.-M. Modeling of power MOSFET for conducting EMI analysis. *J. Zhejiang Univ. Eng. Sci.* **2003**, *37*, 198–214.
2. Abdi, B.; Ranjbar, A.H.; Milimonfared, J.; Gharehpetian, G.B. Reliability comparison of boost PFC converter in DCM and CCM operating modes. In Proceedings of the International Symposium on Power Electronics, Electrical Drives, Automation and Motion, Ischia, Italy, 11–13 June 2008; pp. 939–943.
3. Abdi, B.; Menhaj, M.B.; Yazdanparast, L.; Milimonfared, J. The Effect of the Transformer Winding on the Reliability of Switching Power Supplies. In Proceedings of the 12th International Power Electronics and Motion Control Conference, Portoroz, Slovenia, 30 August–1 September 2006; pp. 663–667.
4. Hirschmann, D.; Tissen, D.; Schroder, S.; de Doncker, R.W. Reliability Prediction for Inverters in Hybrid Electrical Vehicles. *IEEE Trans. Power Electron.* **2007**, *22*, 2511–2517.
5. Zhou, D.; Wang, H.; Blaabjerg, F. Mission Profile based System-level Reliability Analysis of DC/DC Converters for a Backup Power Application. *IEEE Trans. Power Electron.* **2018**, *33*, 8030–8039.
6. Yang, S.; Bryant, A.; Mawby, P.; Xiang, D.; Ran, L.; Tavner, P. An Industry-Based Survey of Reliability in Power Electronic Converters. *IEEE Trans. Ind. Appl.* **2011**, *47*, 1441–1451.
7. Bryant, A.T.; Mawby, P.A.; Palmer, P.R.; Santi, E.; Hudgins, J.L. Exploration of Power Device Reliability using Compact Device Models and Fast Electro-Thermal Simulation. In Proceedings of the Conference Record of the IEEE Industry Applications Conference Forty-First IAS Annual Meeting, Tampa, FL, USA, 8–12 October 2006; pp. 1465–1472.
8. Mahmud, K.; Tao, L. Power factor correction by PFC boost topology using average current control method. In Proceedings of the 2013 IEEE Global High Tech Congress on Electronics, Shenzhen, China, 25–28 October 2013; pp. 16–20.
9. Rajapakse, A.D.; Gole, A.M.; Wilson, P.L. Electromagnetic transient simulation models for accurate representation of switching losses and thermal performance in power electronic systems. *IEEE Trans. Power Deliv.* **2005**, *20*, 319–327.
10. Idir, N.; Bausi`ere, R.; Franchaud, J.J. Active gate voltage control of turn-on di/dt and turn-off dv/dt in insulated gate transistors. *IEEE Trans. Power Electron.* **2006**, *21*, 849–855.
11. Clayton, R.P. *Introduction to Electromagnetic Compatibility*, 2nd ed.; Wiley: Hoboken, NJ, USA, 2006.
12. Liu, Y.; Ravelo, B.; Jastrzebski, A.K. Time-Domain Magnetic Dipole Model of PCB Near-Field Emission. *IEEE Trans. Electromagn. Compat.* **2016**, *58*, 1561–1569.
13. Rajkumar, E.R.; Ravelo, B.; Bensetti, M.; Fernandez-Lopez, P. Application of a hybrid model for the susceptibility of arbitrary shape metallic wires disturbed by EM near-field radiated by electronic structures. *Prog. Electromagn. Res. B* **2012**, *37*, 143–169.
14. Bensetti, M.; Duval, F.; Ravelo, B. Thermal effect modeling on passive circuits with MLP neural network for EMC application. *Prog. Electromagn. Res. M* **2011**, *19*, 39–52.
15. Zhang, R.; Ma, W.; Wang, L.; Hu, M.; Cao, L.; Zhou, H.; Zhang, Y. Line Frequency Instability of One-Cycle-Controlled Boost Power Factor Correction Converter. *Electronics* **2018**, *7*, 203.
16. Kamalpathi, K.; Priyadarshi, N.; Padmanaban, S.; Holm-Nielsen, J.B.; Azam, F.; Umayal, C.; Ramachandaramurthy, V.K. A Hybrid Moth-Flame Fuzzy Logic Controller Based Integrated Cuk Converter Fed Brushless DC Motor for Power Factor Correction. *Electronics* **2018**, *7*, 288.
17. Gorji, S.A.; Mostaan, A.; Ektesabi, M.; Lu, D. A novel bridgeless flyback power factor correction rectifier with single output winding and reduced components voltage stress. In Proceedings of the 19th European Conference on Power Electronics and Applications (EPE'17 ECCE Europe), Warsaw, Poland, 11–14 September 2017; pp. 1–9.
18. Rossetto, L.; Spiazzi, G.; Tenti, P. Control techniques for power factor correction converters. In Proceedings of the Power Electronics Motion Control (PEMC), Warsaw, Poland, 20–22 September 1994.

19. Cuellar, C.; Idir, N.; Benabou, A. High-Frequency Behavioral Ring Core Inductor Model. *IEEE Trans. Power Electron.* **2016**, *31*, 3763–3772.
20. Sullivan, C.R.; Muetze, A. Simulation model of common-mode chokes for high-power applications. *IEEE Trans. Ind. Appl.* **2010**, *46*, 884–891.
21. Cuellar, C.; Tan, W.; Margueron, X.; Benabou, A.; Idir, N. Measurement method of the complex magnetic permeability of ferrites in high frequency. In Proceedings of the IEEE International Instrumentation and Measurement Technology Conference Proceedings, Graz, Austria, 13–16 May 2012; pp. 63–68.
22. Chen, H.L.; Qian, Z.M. High-frequency modeling of common mode chokes for electromagnetic interference analysis. *J. Zhejiang Univ. Eng. Sci.* **2007**, *11*, 1845–1849+1856.



© 2018 by the authors. Submitted for possible open access publication under the terms and conditions of the Creative Commons Attribution (CC BY) license (<http://creativecommons.org/licenses/by/4.0/>).